The Meteoritical Society

Meteoritics & Planetary Science 47, Nr 6, 992–1009 (2012)
doi: 10.1111/j.1945-5100.2012.01366.x

Presolar silicate and oxide abundances and compositions in the ungrouped carbonaceous chondrite Adelaide and the K chondrite Kakangari: The effects of secondary processing

Christine FLOSS* and Frank J. STADERMANN

Laboratory for Space Sciences and Physics Department, Washington University, St. Louis, Missouri 63130, USA
*Corresponding author. E-mail: floss@wustl.edu

(Received 23 September 2011; revision accepted 09 April 2012)

Abstract–Although it has been suggested that the ungrouped carbonaceous chondrite Adelaide and the K chondrite Kakangari could be considered highly primitive, our study of their presolar grain abundances shows that both have experienced more secondary processing than other primitive chondrites with high presolar grain abundances. Presolar grains are rare in Kakangari and are present in reduced abundances in Adelaide (approximately 70 ppm for O-anomalous grains). Thermal annealing has led to widespread crystallization of their fine-grained matrices, and accounts for the partial to complete destruction of presolar grains. In addition, presolar silicates in Adelaide show elevated Fe abundances and Fe-rich rims indicative of infiltration of Fe into the grains from the surrounding matrix. This process probably also took place during annealing, most likely in the solar nebula, in a region with an enhanced dust-to-gas ratio. The most primitive meteorites, with the highest presolar grain abundances, appear to be those whose matrices contain abundant amorphous material that has escaped any significant thermal or aqueous alteration.

INTRODUCTION

In the less than 10 yr since the discovery of presolar silicate grains (e.g., Messenger et al. 2003; Nagashima et al. 2004; Nguyen and Zinner 2004), close to 500 presolar silicates have been identified (Presolar Grain Database: http://presolar.wustl.edu/~pgd) and we have significantly advanced our understanding of their abundances, compositions, and likely origins (Nguyen et al. 2007, 2010; Floss and Stadermann 2009a; Vollmer et al. 2009a; Bose et al. 2010a; Leitner et al. 2012). Presolar silicates are quite abundant, usually about 150–200 ppm in meteorites (Floss and Stadermann 2009a; Vollmer et al. 2009a; Nguyen et al. 2010) and somewhat higher in interplanetary dust particles (IDPs) (e.g., Messenger et al. 2003; Floss et al. 2006; Busemann et al. 2009). The vast majority of presolar silicates have ferromagnesian compositions, and many are either amorphous or complex aggregates of amorphous and nanocrystalline material (Nguyen et al. 2007, 2010; Stroud et al. 2009; Vollmer et al. 2009b). In addition, most have significantly higher Fe contents than expected from condensation under equilibrium conditions (e.g., Lodders and Fegley 1999) and from astronomical observations (e.g., Waters et al. 1996; Demyk et al. 2000). Possible reasons for this have been extensively explored (Floss and Stadermann 2009a; Vollmer et al. 2009a; Bose et al. 2010a) and may include both primary and secondary processes.

Only a handful of the most primitive meteorites contain abundant presolar silicates. In addition to the ungrouped carbonaceous chondrite Acfer 094, the first meteorite in which they were found (Nguyen and Zinner 2004; Nguyen et al. 2007; Vollmer et al. 2009; Bose et al. 2010a), these include the CO3 chondrite ALHA77307 (Nguyen et al. 2010; Bose et al. 2012), and the CR3 chondrites QUE 99177 and MET 00426 (Floss and Stadermann 2009a; Nguyen et al. 2010). Most recently, high abundances of presolar silicates have also been observed in the CO3 chondrite LAP 031117 (Haenecour and Floss 2011) and in the CR chondrite GRV 021710 (Zhao et al. 2011a). Meteorites that have experienced minor secondary processing typically have lower abundances of presolar silicates: for example, the CR2

chondrite NWA 852 has lower presolar silicate abundances (approximately 75 ppm) and a low silicate/oxide ratio, indicating more aqueous alteration than the CR3 chondrites (Leitner et al. 2012). The presolar silicates in these meteorites therefore present opportunities to investigate the effects of secondary processing, in addition to providing information about nucleosynthesis and the stellar environments in which they formed. A special case is represented by the ungrouped C3 chondrite Ningqiang: nominally it has a high presolar silicate abundance (approximately 140 ppm), but almost all the grains were found in a single matrix area; the abundance in this area is about 230 ppm, whereas it is only about 6 ppm for all other areas analyzed in the meteorite (Zhao et al. 2011b).

Adelaide is an ungrouped carbonaceous chondrite, which shows affinities to ALHA77307, but has a significantly higher bulk Fe content (Brearley 1991). Kakangari is the type meteorite for the small K chondrite group, which shows affinities to the other major chondrite groups, but is distinct from all of them: oxygen isotopic compositions are consistent with the CR chondrite group, but bulk elemental compositions are similar to H chondrites and the oxidation state of this grouplet is similar to that of the enstatite chondrites (e.g., Hutchison 2004). Together with Acfer 094 and ALHA77307, these meteorites were characterized as pristine, with abundant primitive matrix material by Scott and Krot (2005) and Nuth et al. (2005). Since Acfer 094 and ALHA77307 both contain high abundances of presolar grains, we initiated a reconnaissance study of Adelaide and Kakangari, in order to assess their presolar grain abundances. Presolar grains were found in abundance in Adelaide, but not in Kakangari. Herein we report detailed results and discuss their significance for understanding secondary processing effects on matrix material in primitive chondrites. Preliminary results were presented by Floss and Stadermann (2009b, 2010).

SAMPLES AND EXPERIMENTAL

We obtained one thin section each of Adelaide (BM1994,M4) and Kakangari (3956-2) from The Natural History Museum (London, UK) and the American Museum of Natural History (New York City, USA), respectively. The samples were documented optically and suitable matrix-rich areas were identified for NanoSIMS analysis. Carbon and O raster ion imaging analyses were carried out using an approximately 1 pA Cs^+ primary beam; secondary ions ($^{12}C^-$, $^{13}C^-$, $^{16}O^-$, $^{17}O^-$, $^{18}O^-$) were collected simultaneously in multicollection mode, along with secondary electrons. Prior to each analysis, a 12×12 μm^2 area was pre-sputtered to remove the C coat. The measurements were carried out by rastering over 10×10 μm^2 areas (256^2 pixels with a dwell time of 20 ms per px) within the pre-sputtered regions, and typically consisted of five layers that were subsequently added together to constitute a single imaging measurement. Multiple sequential analyses were carried out automatically, following a predefined grid pattern.

The data were processed using custom software: isotopic ratio images were calculated after correction for outliers and image shifts between the individual layers of the measurement. Isotopically anomalous grains were identified on the basis of their deviation (at least 5σ) from the average composition of each image and their presence in at least three consecutive layers. Both C and O isotopic compositions were normalized internally, assuming normal bulk isotopic compositions ($^{12}C/^{13}C = 89$; $^{17}O/^{16}O = 3.8 \times 10^{-4}$; $^{18}O/^{16}O = 2.0 \times 10^{-3}$) for the matrix of each meteorite. The total areas measured were 10,000 μm^2 for Kakangari and 34,600 μm^2 for Adelaide (32,300 μm^2 for C, due to a detector malfunction for $^{12}C^-$ in some measurements).

We used the Auger Nanoprobe, operating under our standard conditions for presolar grain analyses (Stadermann et al. 2009), to measure the elemental compositions of the grains: a 10 kV, 0.25 nA primary beam was rastered over the area of each grain and multiple spectra (30–1730 eV) were collected. The spectra were inspected for artifacts and compositional changes during the measurement (which can occur in some labile grains), and were subsequently added together to constitute a single spectrum. Quantitative analyses were obtained for the O-anomalous grains through the use of sensitivity factors determined from olivine and pyroxene standards of various compositions (Stadermann et al. 2009). The reported errors are based on the 1σ uncertainties in the sensitivity factors (O: 3.6%; Si: 11%; Fe: 11.2%; Mg: 9.4%; Ca: 10.8%; Al: 24.9%) and should be considered lower limits, as they do not include a correction for background noise, or take into account other factors that can affect the quality of a spectrum (e.g., sample charging, residual surface contamination). Elemental distribution maps (O, Si, Mg, Fe, Al, Ca, S, C) of the grains and the regions surrounding them were also acquired. Although quantitative data cannot be obtained from these maps, they do provide detailed, qualitative information about the distributions of elements within and around the presolar grains and, in certain cases, can help identify sources of contamination in the spectra (Floss and Stadermann 2009a). Quantitative data were not obtained for the C-anomalous grains, but Auger spectra and maps were used, together with the NanoSIMS data, to identify the grains (e.g., Floss and Stadermann 2009b).

RESULTS AND DATA ANALYSIS

Kakangari

No O-anomalous presolar grains were identified in the 10,000 μm^2 of Kakangari matrix that were analyzed. The upper limit on the abundance of presolar silicates and oxides in this meteorite is about 5 ppm, assuming a presolar grain size of approximately 250 nm. One very small (approximately 200 nm in diameter) C-anomalous grain was found, with a $^{12}C/^{13}C$ ratio of 53 ± 7; the isotopic composition suggests that it is probably SiC. Based on this grain the calculated abundance of SiC in Kakangari is about 4 ppm.

Adelaide—O-anomalous Grains

Table 1 and Fig. 1 show the isotopic compositions of the 56 O-anomalous grains that we found in Adelaide. Grains are identified by the matrix area in which they were measured, followed by the specific raster image within that matrix area, and finally by the grain number. Figure 1 also shows the galactic chemical evolution (GCE) line, which illustrates the expected evolution of oxygen isotopic ratios over galactic history, assuming a constant, solar $^{17}O/^{18}O$ ratio (0.19; Nittler et al. 2008). All but two of the grains have ^{17}O enrichments and solar to subsolar $^{18}O/^{16}O$ ratios (group 1: Nittler et al. 1997); the $^{17}O/^{16}O$ ratio of one of these (5d-17-o1) is 3.4×10^{-3}, similar to the values for "extreme group 1" grains defined by Vollmer et al. (2008). Of the remaining two grains, one is depleted in ^{17}O (group 3) and the other is enriched in ^{18}O (group 4). Elemental compositions are shown in Tables 2 and 3. Forty-two grains are ferromagnesian silicates, nine are oxides and two are complex aggregates of multiple subgrains. The remaining grains could not be analyzed because they sputtered away during the NanoSIMS measurements. Grain sizes are generally less than 350 nm; only one oxide grain (7a-1-o1) and one of the complex grains (3a-1-o2) are larger, with diameters of about half a micrometer (Table 1).

The elemental compositions of the grains can be compared with those of common minerals expected in stellar environments. Figure 2 shows the (Mg + Fe)/Si ratios for the 42 ferromagnesian silicates in Adelaide, compared with the ratios expected for pyroxene (1) and olivine (2), and with similar data for Acfer 094 (Bose et al. 2010a). One grain from Adelaide has a composition consistent with pyroxene, and four others have compositions similar to olivine; cation/O ratios show that all but one of these five grains also have O present in stoichiometric proportions (Table 2). However, the vast majority of the presolar silicates in Adelaide have (Mg + Fe)/Si ratios that are significantly higher than expected for olivine (Fig. 2), and have compositions that do not correspond to any common ferromagnesian minerals. In most cases cation/O ratios are also significantly higher than the ratios expected for pyroxene or olivine (Table 2). However, it should be noted that cation/O ratios are less diagnostic of stoichiometry because residual O from surface contamination may be present in some analyses.

Five of the oxide grains are Al-bearing; all of them also contain Mg and/or Fe (Table 3). Two of them have cation/O ratios consistent with spinel, but the other three do not. Grain 7a-1-o1 has the highest Al concentration of these grains and an Al/O ratio (0.64 ± 0.16) that is close to that of corundum. In principle, it is possible that this is an Al_2O_3 grain, whose spectrum contains some Mg and Fe contamination from the surrounding matrix. However, this seems unlikely for this grain, as it is the largest one in our inventory and there is no obvious evidence for beam shifts during the measurement. Unfortunately, an elemental distribution map, which could help resolve this question, is not available for this grain due to sample charging issues. The remaining four oxide grains are Mg- and/or Fe-bearing. One of these has a stoichiometry consistent with magnesiowüstite [(Mg,Fe)O], but the other three have more O-rich compositions (Table 3).

Finally, two grains consist of aggregates of smaller subgrains. Figure 3 shows isotopic and elemental maps for grain 5a-1-o2. It is about 300 nm in size and consists of two subgrains. The O isotopic composition, which is enriched in ^{17}O and depleted in ^{18}O (group 1), is homogeneous over both subgrains (Fig. 3). The grain to the upper right in Fig. 3 (labeled 1) is a ferromagnesian silicate, while the grain to the lower left (labeled 2) is a Ca,Al-rich oxide (Table 3). The Auger spectra for both grains contain Fe, but the Fe distribution map (Fig. 3) shows the presence of a rim around both grains, with Fe penetrating into the interiors of the grains. If the compositions of the two subgrains are calculated on an Fe-free basis (Table 3), the oxide is compositionally similar to hibonite ($CaAl_{12}O_{19}$), while the silicate has a forsterite (Mg_2SiO_4) composition.

The other complex grain, 3a-1-o2, is somewhat larger, about 500 nm, and shows more structure, in terms of both isotopic and elemental compositions (Figs. 4 and 5). This is also a group 1 grain, but there is some isotopic heterogeneity in the different subgrains of this complex grain. Figure 4 shows the isotopic compositions with three areas labeled, corresponding to three distinct subgrains. The O three isotope plot shows that area 1 is more anomalous than the bulk grain composition, whereas areas 2 and 3 have compositions that are closer to normal (Fig. 4, Table 1). The elemental compositions of the subgrains are shown in Fig. 5 and in

Table 1. Oxygen isotopic compositions of O-anomalous presolar grains in Adelaide.[a]

Grain	$^{17}O/^{16}O$ ($\times10^{-4}$)	$^{18}O/^{16}O$ ($\times10^{-3}$)	Size (nm)	Group	Identification
1a-4-o1	4.84 ± 0.16	1.95 ± 0.03	155	1	Silicate
2a-3-o1	5.80 ± 0.18	2.05 ± 0.03	165	1	Silicate
3a-1-o1	5.37 ± 0.15	2.01 ± 0.03	165	1	Silicate
3a-8-o1	5.61 ± 0.16	1.92 ± 0.03	230	1	Silicate
3b-5-o1	4.99 ± 0.17	1.97 ± 0.03	160	1	Silicate
3c-2-o1	4.91 ± 0.17	1.91 ± 0.03	140	1	Silicate
3c-3-o1	2.86 ± 0.12	1.91 ± 0.03	160	3	Silicate
3c-6-o1	5.11 ± 0.17	1.90 ± 0.03	190	1	Silicate
3c-13-o1	5.66 ± 0.24	1.88 ± 0.04	160	1	Silicate
3d-1-o1	6.11 ± 0.18	1.44 ± 0.03	225	1	Silicate
3d-5-o1	6.33 ± 0.18	1.96 ± 0.03	215	1	Silicate
3e-1o1[d]	5.09 ± 0.17	1.79 ± 0.03	235	1	Not determined
3e-2-o1[d]	5.70 ± 0.17	2.02 ± 0.03	195	1	Not determined
3e-3-o1[d]	5.16 ± 0.16	2.02 ± 0.03	195	1	Not determined
3e-16-o1[d]	5.88 ± 0.18	2.00 ± 0.03	330	1	Not determined
3e-17-o1[d]	8.21 ± 0.23	1.86 ± 0.03	330	1	Not determined
3e-18-o1	8.41 ± 0. 22	1.85 ± 0.03	330	1	Silicate
3e-18-o2	6.58 ± 0. 19	1.94 ± 0.03	250	1	Silicate
3f-9-o1	5.67 ± 0.23	1.62 ± 0.04	230	1	Silicate
3g-1-o1	5.54 ± 0. 23	2.22 ± 0.05	190	1	Silicate
3g-3-o1	5.80 ± 0.24	2.04 ± 0.04	110	1	Silicate
3g-12-o1	5.51 ± 0.25	2.07 ± 0.05	190	1	Silicate
4a-3-o1	5.50 ± 0.23	1.75 ± 0.04	190	1	Silicate
4b-15-o1	4.97 ± 0.18	1.67 ± 0.03	265	1	Silicate
5a-1-o1	13.2 ± 0.3	2.05 ± 0.03	325	1	Silicate
5a-5-o2	5.29 ± 0.22	1.75 ± 0.04	275	1	Silicate
5a-12-o1	5.42 ± 0.20	1.55 ± 0.03	255	1	Silicate
5a-13-o1	5.24 ± 0.16	2.03 ± 0.03	155	1	Silicate
5a-18-o1	6.80 ± 0.20	1.71 ± 0.03	205	1	Silicate
5c-1-o1	5.20 ± 0.22	1.92 ± 0.04	275	1	Silicate
5c-3-o1	11.4 ± 0.3	1.83 ± 0.04	300	1	Silicate
5c-10-o1	9.38 ± 0.28	1.74 ± 0.03	355	1	Silicate
5d-6-o1	6.21 ± 0.19	2.04 ± 0.03	275	1	Silicate
5d-7-o1	5.84 ± 0.21	1.85 ± 0.04	215	1	Silicate
5d-13-o1	5.53 ± 0.21	2.04 ± 0.04	240	1	Silicate
5d-13-o2	5.38 ± 0.21	2.00 ± 0.04	265	1	Silicate
5d-13-o3	4.61 ± 0.20	1.73 ± 0.04	175	1	Silicate
5d-14-o1	4.81 ± 0.20	2.05 ± 0.04	220	1	Silicate
5d-17-o1	33.8 ± 0.5	1.92 ± 0.04	180	1x[b]	Silicate
5d-18-o1	10.7 ± 0.3	2.01 ± 0.04	200	1	Silicate
5e-1-o1	4.84 ± 0.23	1.97 ± 0.05	185	1	Silicate
5e-7-o1	6.80 ± 0.31	1.23 ± 0.04	285	1	Silicate
5e-7-o2	5.40 ± 0.22	1.97 ± 0.04	195	1	Silicate
6a-2-o1	8.03 ± 0.36	1.84 ± 0.05	315	1	Silicate
6a-8-o1	4.80 ± 0.26	1.96 ± 0.05	165	1	Silicate
6b-10-o1	3.73 ± 0.20	2.82 ± 0.05	230	4	Silicate
9a-6-o1	5.54 ± 0.18	1.87 ± 0.03	255	1	Silicate
3a-1-o2[c]	4.42 ± 0.10	1.78 ± 0.02	480	1	Complex
Area 1	4.60 ± 0.16	1.67 ± 0.03		1	Oxide
Area 2	4.36 ± 0.14	1.78 ± 0.03		1	Oxide
Area 3	4.25 ± 0.23	1.82 ± 0.04		1	Oxide
5a-1-o2	5.47 ± 0.19	1.54 ± 0.03	315	1	Complex
3c-13-o2	5.92 ± 0.19	1.97 ± 0.03	145	1	Oxide
3g-13-o1	4.96 ± 0.14	1.74 ± 0.03	165	1	Oxide
4b-7-o1	4.83 ± 0.19	1.59 ± 0.04	230	1	Oxide

Table 1. *Continued*. Oxygen isotopic compositions of O-anomalous presolar grains in Adelaide.

Grain	$^{17}O/^{16}O$ ($\times 10^{-4}$)	$^{18}O/^{16}O$ ($\times 10^{-3}$)	Size (nm)	Group	Identification
4b-16-o1	5.01 ± 0.19	1.91 ± 0.04	205	1	Oxide
5a-5-o1	6.17 ± 0.24	2.15 ± 0.04	225	1	Oxide
5a-19-o1	6.45 ± 0.20	2.08 ± 0.03	205	1	Oxide
5b-1-o1	5.84 ± 0.17	1.86 ± 0.03	195	1	Oxide
5d-17-o2	6.53 ± 0.23	2.03 ± 0.04	215	1	Oxide
7a-1-o1	15.7 ± 0.2	1.88 ± 0.02	570	1	Oxide

[a]Errors are 1σ.
[b]Extreme group 1.
[c]Average composition for the whole grain and for three areas with different isotopic compositions.
[d]Grain sizes determined from NanoSIMS images.

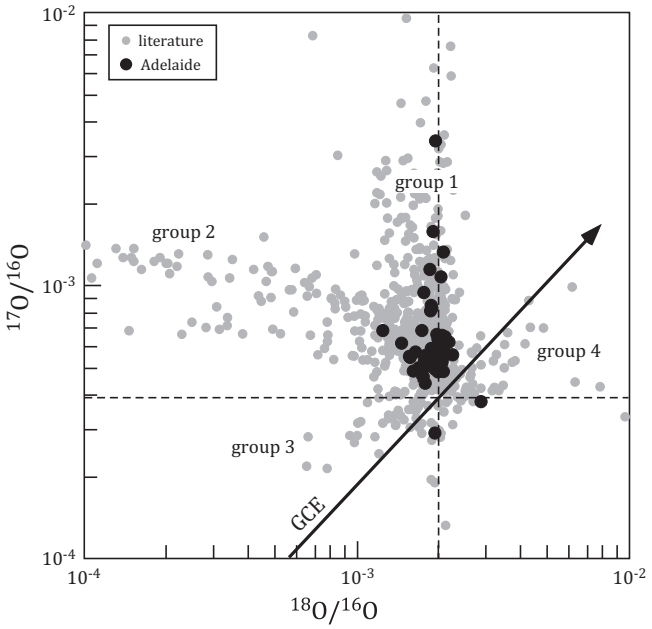

Fig. 1. Oxygen three isotope plot showing O-anomalous grains in Adelaide. GCE: Galactic Chemical Evolution line; see text. Group designations are based on Nittler et al. (1997). Literature data are from the Presolar Grain Database (http://presolar.wustl.edu/~pgd).

Table 3. The grain corresponding to area 1 is dominated by Al and has a lower portion that also contains Ca. This central Al-rich area is rimmed on the bottom by Fe,Mg-oxide grains that correspond to areas 2 and 3. Here too, the Fe distribution map shows Fe penetrating the Al-rich core grain. On an Fe-free basis, the Al-rich core is stoichiometrically similar to corundum (Al_2O_3) and the Ca-bearing portion has a composition consistent with grossite ($CaAl_4O_7$). However, it is less clear whether the Fe in the Fe,Mg-oxides is intrinsic to the grains or whether there is a contribution from the surrounding matrix. These grains have variable, nonstoichiometric compositions.

Adelaide—C-anomalous Grains

We identified 13 C-anomalous grains in Adelaide (Table 4). Seven of these are mainstream SiC and two are A + B grains with very low $^{12}C/^{13}C$ ratios. The other four C-anomalous grains could not be measured in the Auger Nanoprobe, either due to charging issues or because they sputtered away during the NanoSIMS measurement. Based on its isotopic composition, grain 3e-3-c1 is probably a mainstream SiC. The other three grains have $^{12}C/^{13}C$ ratios that are higher than solar. The $^{12}C^-/^{16}O^-$ ratios obtained from the NanoSIMS measurements are not very diagnostic, but they are within the ranges obtained from the identified SiC grains (0.01–0.06), whereas $^{12}C^-/^{16}O^-$ ratios for other C-rich areas in the NanoSIMS images are typically about an order of magnitude higher. If these grains are SiC, they could be either X or Y grains. However, we cannot rule out the possibility that they are graphite or some other carbonaceous phase.

Adelaide—NanoSIMS Depth Profile

Due to an error in software input during one NanoSIMS measurement run, rather than measuring in a grid pattern over an area of matrix, a sequence of 18 imaging measurements were acquired over the same 10 × 10 μm^2 area. These unintended sequential measurements provide a depth profile through the thin section and allow changes in the matrix to be examined in the third dimension. Within these 18 measurements, we identified four distinct O-anomalous grains (Table 1) and two C-anomalous grains (Table 4); these grains are labeled with the prefix "3e" in Tables 1 and 4. Two of the O-anomalous grains are present in more than one measurement: 3e-2-o1 and 3e-3-o1 are the same grain (3e-A) tracked through measurements 2 and 3; and 3e-16-o1, 3e-17-o1, and 3e-18-o1 are one grain (3e-B), tracked through the final three measurements. For grain 3e-B the isotopic composition in the first measurement (3e-16-o1) is somewhat less anomalous than the other two. This is due to a higher

Table 2. Elemental compositions (atom%) of presolar silicate grains in Adelaide[a]

	O	Si	Mg	Fe	Al	Ca	(Fe + Mg)/Si	Cation/O	Mg[b]
Silicates									
1a-4-o1	44.9 ± 1.6	12.5 ± 1.4	5.1 ± 0.5	37.6 ± 4.2			3.4 ± 0.5	1.23 ± 0.11	11.9
2a-3-o1	44.1 ± 1.6	12.3 ± 1.4	7.9 ± 0.7	35.8 ± 4.0			3.6 ± 0.5	1.27 ± 0.11	18.0
3a-1-o1	57.1 ± 2.1	11.0 ± 1.2	6.9 ± 0.7	25.0 ± 2.8			2.9 ± 0.4	0.75 ± 0.06	21.8
3a-8-o1	47.3 ± 1.7	10.0 ± 1.1	5.6 ± 0.5	37.1 ± 4.2			4.2 ± 0.6	1.12 ± 0.10	13.1
3b-5-o1	42.6 ± 1.5	14.1 ± 1.6	8.9 ± 0.8	34.4 ± 3.9			3.1 ± 0.4	1.35 ± 0.11	20.6
3c-2-o1	44.8 ± 1.6	12.6 ± 1.4	5.0 ± 0.5	31.3 ± 3.5	6.4 ± 1.6		2.9 ± 0.4	1.23 ± 0.10	13.9
3c-6-o1	50.9 ± 1.8	14.5 ± 1.6	16.5 ± 1.6	18.1 ± 2.0			2.4 ± 0.3	0.97 ± 0.07	47.6
3c-13-o1	38.5 ± 1.4	14.8 ± 1.6	5.1 ± 0.5	41.6 ± 4.7			3.2 ± 0.5	1.60 ± 0.14	11.0
3d-1-o1	47.6 ± 1.7	13.9 ± 1.5	24.2 ± 2.3	14.4 ± 1.6			2.8 ± 0.4	1.10 ± 0.08	62.7
3d-5-o1	37.6 ± 1.4	14.4 ± 1.6	7.5 ± 0.7	40.5 ± 4.5			3.3 ± 0.5	1.66 ± 0.14	15.6
3e-18-o1	48.2 ± 1.7	13.0 ± 1.4	15.1 ± 1.5	23.1 ± 2.6			3.0 ± 0.4	1.08 ± 0.08	40.4
3e-18-o2	44.1 ± 1.6	15.4 ± 1.7	13.1 ± 1.2	27.4 ± 3.1			2.6 ± 0.4	1.27 ± 0.10	32.3
3f-9-o1	48.3 ± 1.7	14.9 ± 1.6	15.8 ± 1.5	21.0 ± 2.4			2.5 ± 0.3	1.07 ± 0.08	42.9
3g-1-o1	55.3 ± 2.0	10.2 ± 1.1	11.9 ± 1.1	22.6 ± 2.5			3.4 ± 0.5	0.81 ± 0.06	34.5
3g-3-o1	54.0 ± 1.9	12.1 ± 1.3	8.0 ± 0.8	25.9 ± 2.9			2.8 ± 0.4	0.85 ± 0.07	23.5
3g-12-o1	50.8 ± 1.8	14.3 ± 1.6	10.1 ± 1.0	24.8 ± 2.8			2.4 ± 0.3	0.97 ± 0.07	28.9
4a-3-o1	60.2 ± 2.2	8.3 ± 0.9	11.2 ± 1.1	20.3 ± 2.3			3.8 ± 0.5	0.66 ± 0.05	35.5
4b-15-o1	55.3 ± 2.0	9.3 ± 1.0	5.8 ± 0.5	29.6 ± 3.3			3.8 ± 0.6	0.81 ± 0.07	16.3
5a-1-o1	52.7 ± 1.9	9.7 ± 1.1	8.4 ± 0.8	29.2 ± 3.3			3.9 ± 0.5	0.90 ± 0.07	22.4
5a-5-o2	52.9 ± 1.9	12.1 ± 1.3	24.7 ± 2.3	10.3 ± 1.2			2.9 ± 0.4	0.89 ± 0.06	70.7
5a-12-o1	38.5 ± 1.4	11.8 ± 1.3	8.3 ± 0.8	41.5 ± 4.6			4.2 ± 0.6	1.60 ± 0.14	16.7
5a-13-o1	52.4 ± 1.9	8.2 ± 0.9	5.4 ± 0.5	34.1 ± 3.8			4.8 ± 0.7	0.91 ± 0.08	13.6
5a-18-o1	42.9 ± 1.5	13.9 ± 1.5	14.8 ± 1.4	28.5 ± 3.2			3.1 ± 0.4	1.33 ± 0.10	34.2
5c-1-o1	52.0 ± 1.9	11.8 ± 1.3	9.2 ± 0.9	26.9 ± 3.0			3.1 ± 0.4	0.92 ± 0.07	25.5
5c-3-o1	52.7 ± 1.9	10.7 ± 1.2	10.4 ± 1.0	26.2 ± 2.9			3.4 ± 0.5	0.90 ± 0.07	28.4
5c-10-o1	49.9 ± 1.8	13.2 ± 1.5	13.9 ± 1.3	23.0 ± 2.6			2.8 ± 0.4	1.00 ± 0.07	37.8
5d-6-o1	53.8 ± 1.9	10.3 ± 1.1	11.5 ± 1.1	24.4 ± 2.7			3.5 ± 0.5	0.86 ± 0.07	32.0
5d-7-o1	53.2 ± 1.9	7.1 ± 0.8	13.7 ± 1.3	26.0 ± 2.9			5.6 ± 0.8	0.88 ± 0.07	34.6
5d-13-o1	48.3 ± 1.7	15.2 ± 1.7	10.3 ± 1.0	26.3 ± 2.9			2.4 ± 0.3	1.07 ± 0.08	28.1
5d-13-o3	49.2 ± 1.8	11.5 ± 1.3	11.0 ± 1.0	28.3 ± 3.2			3.4 ± 0.5	1.03 ± 0.08	28.0
5d-14-o1	52.7 ± 1.9	11.1 ± 1.2	12.2 ± 1.2	24.1 ± 2.7			3.3 ± 0.4	0.90 ± 0.07	33.6
5d-17-o1	53.3 ± 1.9	12.0 ± 1.3	11.3 ± 1.1	23.4 ± 2.6			2.9 ± 0.4	0.88 ± 0.07	32.5
5d-18-o1	50.1 ± 1.8	12.5 ± 1.4	9.5 ± 0.9	27.9 ± 3.1			3.0 ± 0.4	1.00 ± 0.08	25.4
5e-1-o1	52.0 ± 1.9	11.0 ± 1.2	9.6 ± 0.9	27.3 ± 3.1			3.4 ± 0.5	0.92 ± 0.07	26.1
5e-7-o1	52.7 ± 1.9	13.8 ± 1.5	15.4 ± 1.4	18.2 ± 2.0			2.4 ± 0.3	0.90 ± 0.06	45.7
5e-7-o2	49.0 ± 1.8	12.9 ± 1.4	7.3 ± 0.7	30.9 ± 3.5			3.0 ± 0.4	1.04 ± 0.09	19.1
6b-10-o1	55.1 ± 2.0	12.7 ± 1.4	6.8 ± 0.6	25.4 ± 2.8			2.5 ± 0.4	0.82 ± 0.07	21.2
3c-3-o1	58.2 ± 2.1	22.9 ± 2.5	15.6 ± 1.5	3.3 ± 0.4			0.8 ± 0.1	0.72 ± 0.06	82.6
5d-13-o2	51.4 ± 1.9	16.0 ± 1.8	12.3 ± 1.2	20.3 ± 2.3			2.0 ± 0.3	0.95 ± 0.07	37.8
6a-2-o1	57.6 ± 2.1	15.2 ± 1.7	15.1 ± 1.4	12.1 ± 1.4			1.8 ± 0.2	0.74 ± 0.05	55.6
6a-8-o1	54.9 ± 2.0	15.2 ± 1.7	8.6 ± 0.8	21.4 ± 2.4			2.0 ± 0.3	0.82 ± 0.06	28.5
9a-6-o1	56.7 ± 2.0	15.6 ± 1.7	10.7 ± 1.0	17.0 ± 1.9			1.8 ± 0.2	0.76 ± 0.06	38.6
Pyroxene	$(Mg,Fe)SiO_3$						1 (stds: 1.0–1.3)	0.67 (stds: 0.59–0.78)	
Olivine	$(Mg,Fe)_2SiO_4$						2 (stds: 1.8–2.1)	0.75 (stds: 0.61–0.93)	

[a]Errors are 1σ.
[b][(Mg + Fe)/Mg]*100.

degree of dilution with isotopically normal oxygen as the beam begins to sputter through the overlying matrix to the grain; the grain composition becomes steadily more anomalous through the different layers of this measurement and in the final layer is similar to the average compositions recorded for 3e-17-o1 and 3e-18-o1.

The presence of these grains in multiple sequential images can be used to estimate a sputtering rate for the NanoSIMS measurements and, thereby, can provide an estimate of what fraction of a typical presolar grain is left at the end of one of our NanoSIMS measurements. Grain 3e-A is present in a total of seven layers in the two

Table 3. Elemental compositions (atom%) of presolar oxide and complex grains in Adelaide.[a]

	O	Si	Mg	Fe	Al	Ca	(Fe + Mg)/Si	Cation/O
Oxides								
3c-13-o2	50.5 ± 1.8		4.7 ± 0.4	44.9 ± 5.0				0.98 ± 0.11
3g-13-o1	57.1 ± 2.1		7.4 ± 0.7	15.7 ± 1.8	19.9 ± 4.9			0.75 ± 0.10
4b-7-o1	56.7 ± 2.0			24.8 ± 2.8	18.5 ± 4.6			0.76 ± 0.10
4b-16-o1	57.2 ± 2.1			42.8 ± 4.8				0.75 ± 0.09
5a-5-o1	51.2 ± 1.8		6.0 ± 0.6	15.3 ± 1.7	27.6 ± 6.9			0.95 ± 0.14
5a-19-o1	50.7 ± 1.8		9.3 ± 0.9	16.0 ± 1.8	24.0 ± 6.0			0.97 ± 0.13
5b-1-o1	58.0 ± 2.1		8.3 ± 0.8	33.8 ± 3.8				0.73 ± 0.07
5d-17-o2	56.7 ± 2.0		9.4 ± 0.9	33.9 ± 3.8				0.76 ± 0.07
7a-1-o1	50.8 ± 1.8		8.0 ± 0.8	8.6 ± 1.0	32.7 ± 8.1			0.97 ± 0.17
7a-1-o1[b]	60.9 ± 2.2				39.1 ± 9.8			0.64 ± 0.16
Corundum	Al_2O_3							*0.67*
Spinel	$MgAl_2O_4$							*0.75*
Hibonite	$CaAl_{12}O_{19}$							*0.68*
Complex Grains								
3a-1-o2								
Grain 1a	52.2 ± 1.9			13.0 ± 1.5	33.9 ± 8.4			0.90 ± 0.17
Grain 1a[b]	60.0 ± 2.2				40.0 ± 10.0			0.67 ± 0.17
Grain 1b	48.5 ± 1.7			14.6 ± 1.6	28.4 ± 7.1	8.5 ± 0.9		1.06 ± 0.16
Grain 1b[b]	56.8 ± 2.0				33.3 ± 8.3	10.0 ± 1.1		0.76 ± 0.15
Grain 2	52.8 ± 1.9		21.0 ± 2.0	26.2 ± 2.9				0.90 ± 0.07
Grain 3	55.6 ± 2.0		16.8 ± 1.6	27.6 ± 3.1				0.80 ± 0.07
5a-1-o2								
Grain 1	52.5 ± 1.9	9.9 ± 1.1	20.0 ± 1.9	17.6 ± 2.0			3.8 ± 0.5	0.90 ± 0.06
Grain 1[b]	53.9 ± 1.9	15.2 ± 1.7	30.9 ± 3.4				2.0 ± 0.3	0.86 ± 0.08
Grain 2	52.9 ± 1.9			25.5 ± 0.9	19.6 ± 0.7	1.94 ± 0.07		0.89 ± 0.04
Grain 2[b]	56.1 ± 2.0				40.0 ± 10.0	4.0 ± 0.4		0.78 ± 0.18

[a]Errors are 1σ.
[b]Recalculated with no Fe; see text for details.

measurements (layers 2-5 in 3e-2-o1 and layers 1-3 in 3e-3-o1). With a dwell time of 20 ms per px, each layer takes just under 22 min to complete. Assuming a spherical grain, with a maximum diameter of 195 nm (Table 1), the average sputtering rate is about 1.3 nm min^{-1}. Grain 3e-B, which is a ferromagnesian silicate (Table 2), is 330 nm in diameter and is present in all 15 layers of the three measurements in which it was identified. Since some unknown fraction of this grain was not sputtered away, the average sputtering rate obtained from grain 3e-B, about 1.0 nm min^{-1}, is an upper limit. The remaining O-anomalous grain and the C-anomalous grains are each present only in the five layers of one image of their respective measurements. Grain 3e-1o-1 has a diameter of 235 nm (Table 1) and a calculated sputtering rate of about 2.0 nm min^{-1}. Grains 3e-3-c1 and 3e-7-c1 have diameters of 155 and 330 nm, respectively; their respective calculated sputtering rates are about 1.4 nm min^{-1} and about 3.0 nm min^{-1}. Sputtering rates will be variable, depending on the material being sputtered and the measurement conditions being used (e.g., primary beam current), but in addition, the assumption of a spherical grain shape may not be valid for all grains and a nonspherical grain geometry will clearly affect calculated sputtering rates. However, these data suggest that under the conditions normally used for our presolar grain searches, about half of a typical approximately 250 nm presolar silicate grain should be left at the end of an imaging measurement. This is consistent with our observation that few grains are completely sputtered away at the end of our measurements.

DISCUSSION

Isotopic Compositions and Origins of O-Anomalous Grains

As in other presolar grain-rich primitive meteorites, most of the O-anomalous grains in Adelaide belong to group 1 (Fig. 1). These grains probably originated in O-rich low-mass (approximately 1.2–2.2 $M_\odot$) red giant or asymptotic giant branch (AGB) stars with close to solar metallicity (Nittler et al. 1997, 2008); the first dredge-up after hydrogen burning increases the $^{17}O/^{16}O$ ratio in the stellar envelope where grains form, but has little effect on the $^{18}O/^{16}O$ ratio, which is largely determined by the initial metallicity of the star. The high abundance of

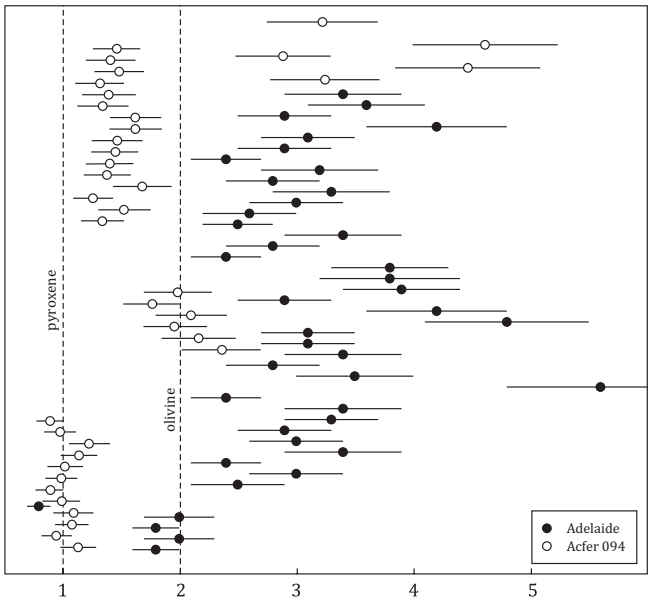

Fig. 2. Plot of (Fe + Mg)/Si ratios in ferromagnesian silicates from Adelaide and Acfer 094. Errors are 1σ. Data for Acfer 094 are from Bose et al. (2010a). Data are not shown for the complex grains from Adelaide and a few unusual grains in Acfer 094 with ratios < 1.

group 1 grains is in good agreement with recent modeling work carried out by Gail et al. (2009), which shows that a large fraction of the O-rich dust contributed to our solar nebula originated in low-mass thermally pulsing AGB stars of close to solar metallicity. Their model also predicts that about half of the O-rich dust should come from more massive (approximately 4–8 M€) AGB stars, but grains with the isotopic signatures of hot bottom burning expected from such stars (Iliadis et al. 2008) are not present in the presolar grain population. At present there is no satisfactory resolution to this discrepancy. Gail et al. (2009) suggested nonhomogeneous distribution of stellar grains to the solar system as a possibility, whereas Nittler (2009) noted that the amount of hot bottom burning predicted to occur in intermediate mass stars of solar metallicity may be overestimated.

Dredge-up cannot account for the isotopic compositions of group 1 grains with very high $^{17}O/^{16}O$ ratios. Calculations by Boothroyd and Sackmann (1999) indicated a limit on the $^{17}O/^{16}O$ ratio of approximately 4×10^{-3} for low to intermediate mass stars of close-to-solar metallicity. However, recent calculations using a revised estimate of the solar metallicity and new reaction rates that are important for the CNO cycle suggest somewhat higher limits of approximately 6×10^{-3} (Gyngard et al. 2011). One of our grains (5d-17-o1) has a $^{17}O/^{16}O$ ratio of 33.8×10^{-4}. Dilution from surrounding isotopically normal grains is known to have a significant effect on the isotopic compositions of presolar grains

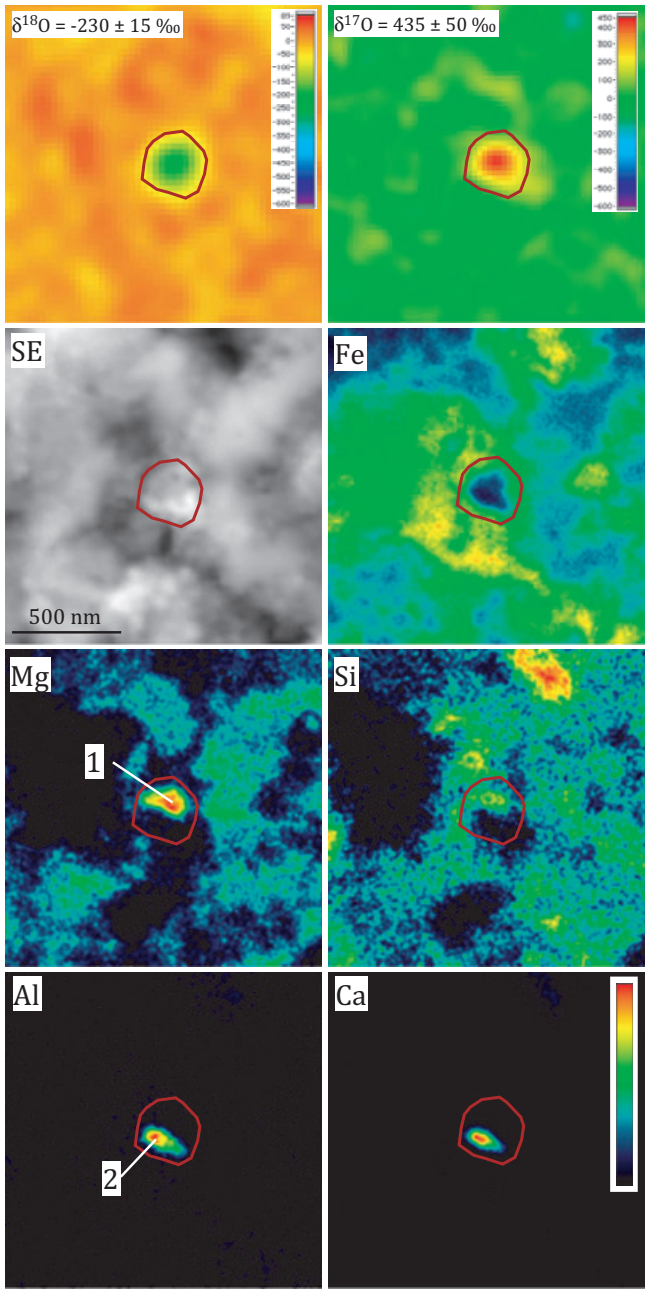

Fig. 3. Secondary electron, and false-color isotopic and elemental images of complex grain 5a-1-o2. The isotopic compositions in the two images at the top are expressed in delta notation: $[((R_{sample}/R_{standard}) - 1))*1000]$. The area of the isotopic anomaly is outlined in red and the two subgrains are labeled.

identified through raster ion imaging (Nguyen et al. 2007), and the effect is most pronounced for the smallest grains. Grain 5d-17-o1 has a diameter of only 180 nm and its true isotopic composition is almost certainly above the first dredge-up limit; calculations by Nguyen et al. (2007) suggest dilution by a factor of 2–3 for a grain of this size, which would imply a true isotopic

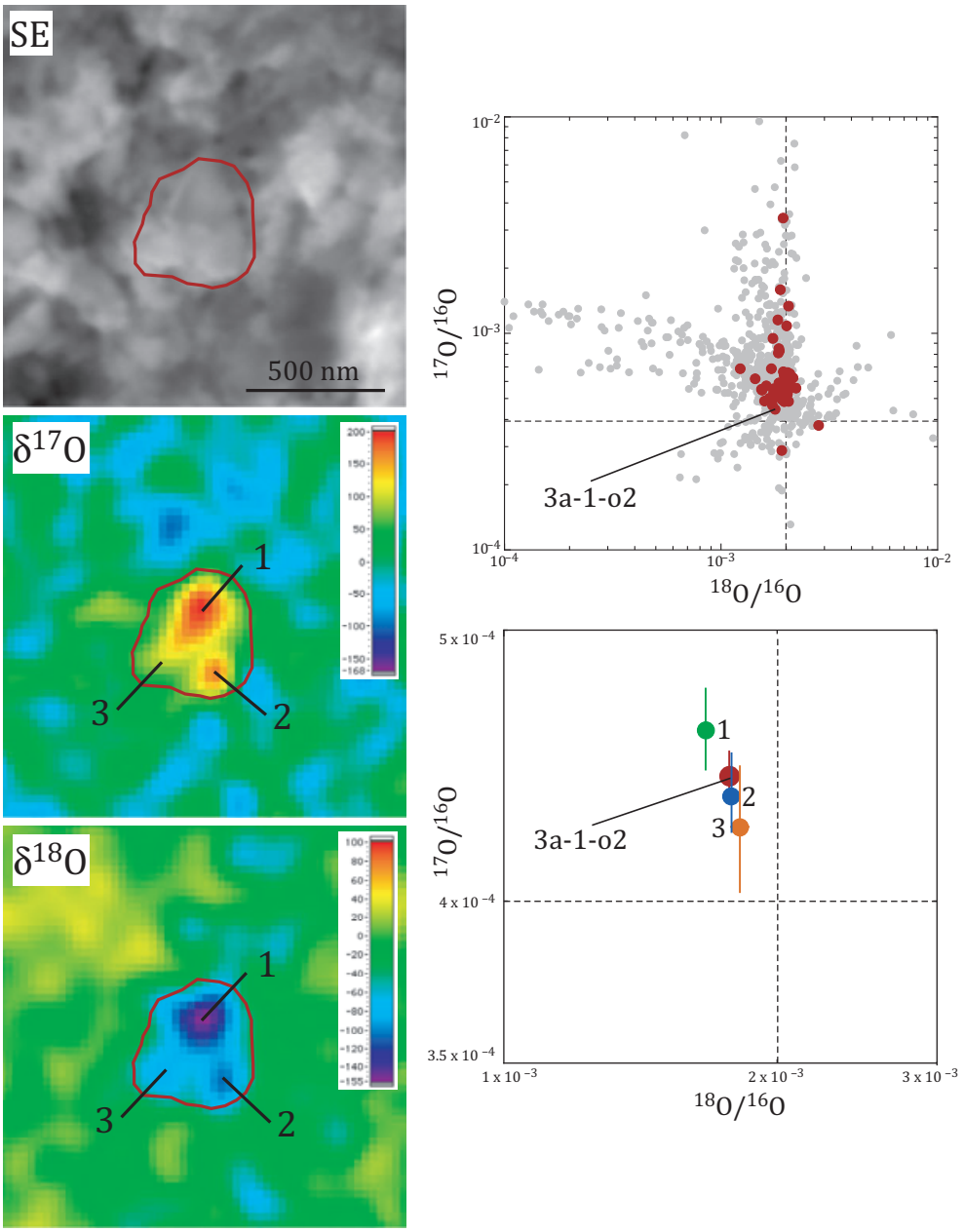

Fig. 4. Oxygen isotopic compositions of complex grain 3a-1-o2. The secondary electron image and false-color isotopic images (in delta notation) show the grain outlined in red; three areas with distinct O isotopic compositions are labeled in the images and are shown, along with the average composition of the grain, in the O three isotope plots.

composition of approximately $7–10 \times 10^{-3}$. Vollmer et al. (2008) also identified several "extreme" group 1 grains with isotopic compositions similar to our grain. Nittler and Hoppe (2005) suggested that grains with very high $^{17}O/^{16}O$ ratios could have a nova origin. Early model predictions for novae of various stellar masses (e.g., José et al. 2004) were consistent with the O isotopic compositions of extremely ^{17}O-enriched grains such as T54 (Nittler et al. 1997). However, updated calculations with new reaction rates indicate that the predicted O isotopic compositions do not match the grain data unless large amounts of mixing with solar composition matter is included (Gyngard et al. 2010, 2011). Isotopic data for other elements (e.g., Si, Mg) in a few extreme group 1 grains indicate similar large discrepancies (Vollmer et al. 2008; Gyngard et al. 2010, 2011). An alternate possibility is that mass loss to a binary companion could diminish the envelope of a main sequence star, with the result that the ^{17}O brought to the envelope during the first dredge-up is less diluted, leading to more elevated $^{17}O/^{16}O$ ratios

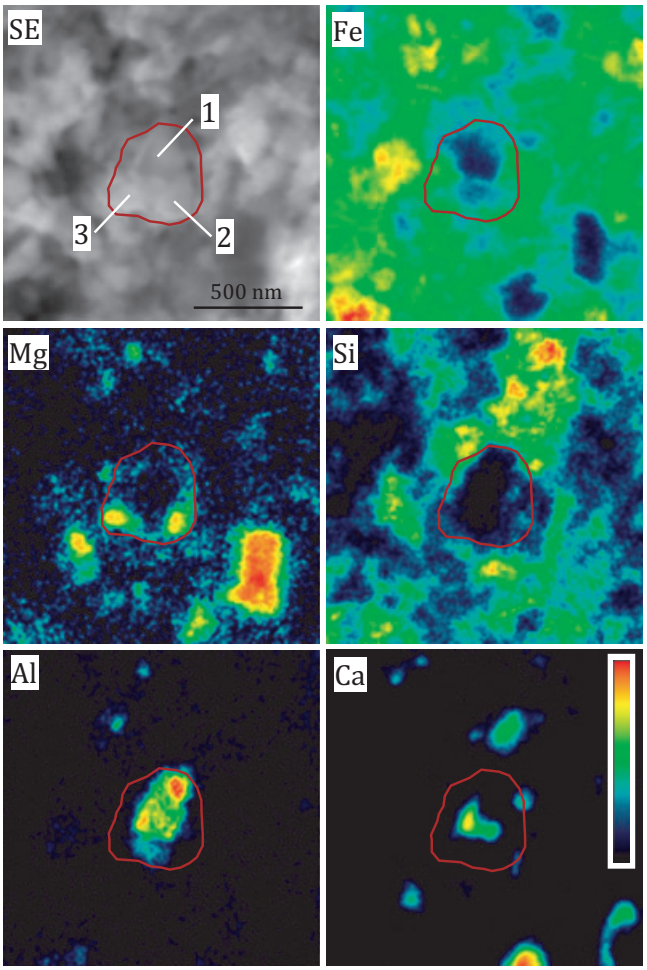

Fig. 5. Secondary electron and false-color elemental images of complex grain 3a-1-o2. The area of the anomaly is outlined in red and the three subgrains are labeled.

than normally expected from this process (Nittler et al. 2008). Clearly, additional data and modeling efforts are needed to understand the origin of these grains.

One group 3 grain and one group 4 grain are also present in our inventory. The group 3 grain is depleted in ^{17}O, with solar $^{18}O/^{16}O$ and plots below the GCE line, whereas the group 4 grain is enriched in ^{18}O, with solar $^{17}O/^{16}O$ (Fig. 1). The isotopic compositions of group 3 grains, which plot below the GCE line, cannot be explained by dredge-up in AGB stars unless they originated in stars with lower than solar $^{17}O/^{18}O$ ratios, which is unlikely since the solar $^{17}O/^{18}O$ ratio is already low relative to typical molecular clouds in the Milky Way (Wilson and Rood 1994). Nittler et al. (2008) suggested that such group 3 grains, along with ^{18}O-rich group 4 grains, could have a supernova origin, as their isotopic compositions fall along a mixing line of ^{16}O-rich material from the supernova interior and material from the He/C and He/N zones, and the H envelope. These

Table 4. Carbon-anomalous grains in Adelaide.[a]

Grain	$^{12}C/^{13}C$	Size (nm)	Identification
3c-6-c1	70.5 ± 1.6	175	SiC (ms)
3c-15-c1	2.8 ± 0.1	160	SiC (A + B)
3g-20-c1	17.3 ± 0.4	85	SiC (ms)
4b-6-c1	22.0 ± 0.5	230	SiC (ms)
5a-4-c1	70.2 ± 2.5	180	SiC (ms)
5a-10-c1	45.7 ± 3.3	255	SiC (ms)
5a-12-c1	55.9 ± 3.9	160	SiC (ms)
5b-2-c1	6.6 ± 0.1	135	SiC (A + B)
8a-1-c1	68.3 ± 1.4	230	SiC (ms)
3e-3-c1[b]	50.6 ± 2.6	155	Not determined
3e-7-c1[b]	111 ± 3	330	Not determined
5c-3-c1	133 ± 8	110	Not determined
9a-11-c1	118 ± 3	235	Not determined

[a]Errors are 1σ.
[b]Grain sizes determined from NanoSIMS images.
ms = mainstream.

authors noted, furthermore, that the fact that most group 4 (and some group 3) grains are broadly consistent with a single mixing line could indicate their origin from a single nearby supernova, possibly one triggering collapse of the molecular cloud from which the solar system originated. Group 4 grains normally make up about 10% of the presolar silicate and oxide population. However, in Adelaide the single group 4 grain represents only 2% of the O-anomalous grains identified. Yada et al. (2008) noted that group 4 grains were significantly more abundant in IDPs and Antarctic micrometeorites (approximately 35%) than in the overall presolar silicate and oxide population. If these grains were injected into the early solar nebula by a supernova, such differences could indicate formation of the respective parent bodies at different times or in different parts of the nebula (Yada et al. 2008).

Isotopic Compositions and Origins of C-Anomalous Grains

The majority of the C-anomalous grains in Adelaide have $^{12}C/^{13}C$ ratios between 10 and 100 and are likely to be mainstream SiC grains (although in the absence of additional isotopic data we cannot rule out the possibility that some of them are X or Z grains); the origin of these grains in C-rich AGB stars is well established, although their Si isotopic compositions remain unexplained (e.g., Zinner 2007). Our inventory also includes two A + B grains (Table 4), defined as those grains with $^{12}C/^{13}C$ ratios of less than 10 (Amari et al. 2001). These grains make up about 4–5% of the SiC population, but remain poorly understood. J-type carbon stars with low $^{12}C/^{13}C$ ratios are one likely source; A + B grains with enhanced abundances of s-process grains may also come from born-again AGB

stars, such as Sakurai's object (Amari et al. 2001). However, the large spread in $^{14}N/^{15}N$ ratios exhibited by these grains is not well understood (Zinner 2007).

Finally, the elemental compositions of four C-anomalous grains could not be determined; one of these is probably a mainstream grain, based on its $^{12}C/^{13}C$ ratio. The isotopic compositions of the other three grains, with elevated $^{12}C/^{13}C$ ratios, are consistent with X or Y grains. However, these groups each make up only about 1% of the SiC population, and it seems unlikely that we would find three such grains in this limited inventory of C-anomalous grains. Graphite grains have higher than solar $^{12}C/^{13}C$ ratios, but abundances of presolar graphite are lower than most other presolar grain types (Zinner 2007) and, therefore, like X or Y grains, we would not expect to find many graphite grains in our C-anomalous grain inventory. A final possibility is that these are carbonaceous grains of interstellar or cold molecular cloud origin, similar to grains with ^{13}C depletions that have been found in some primitive meteorites and IDPs (Floss et al. 2004, 2006, 2010; Floss and Stadermann 2009c). However, these phases appear to be highly susceptible to thermal processing and are only found in the most primitive extraterrestrial materials. As discussed in more detail below, Adelaide appears to have experienced some metamorphism, which such grains are unlikely to have survived. With no additional elemental or isotopic information, it is difficult to say more about the nature of these three C-anomalous grains.

Complex Grains 3a-1-o2 and 5a-1-o2

The isotopic compositions of both complex grains (group 1) indicate that they formed in low-mass red giant or AGB stars with close to solar metallicity. Refractory Al-bearing oxides, such as the ones in 3a-1-o2 and 5a-1-o2, tend to form in stars with low-mass loss rates in the early AGB phase (e.g., Sloan et al. 2003; Maldoni et al. 2008) and are also the first solids expected to condense from an O-rich circumstellar gas (Lodders and Fegley 1999). Fe,Mg-oxides, like those present in 3a-1-o2, are also expected to form in O-rich AGB stars with low-mass loss rates (Gail and Sedlmayr 1999; Ferrarotti and Gail 2001). At higher mass-loss rates, silicate condensation is dominant, and olivine is the first phase to form (Ferrarotti and Gail 2001). As temperatures decrease following the initial condensation of corundum, this phase can react with the gas to form other phases, such as grossite, hibonite, or Al-bearing silicates, or can act as a nucleation site for the subsequent condensation of ferromagnesian silicates (Gail and Sedlmayr 1999; Demyk et al. 2000; Toppani et al. 2006).

Grain 5a-1-o2 consists of a forsterite-like silicate and a hibonite-like grain. Although the hibonite-like grain probably formed before the silicate, it is not clear from the texture of this compound grain (Fig. 3) whether it acted as a nucleation site for the silicate, or whether the two subgrains formed independently. The homogeneous O isotopic composition of the compound grain does argue for aggregation of the two subgrains in the same stellar environment, and indicates that, despite the difference in elemental compositions, there was no substantial change in the O isotopic composition of the gas during condensation of these components. Grain 3a-1-o2 is an aggregate of Al_2O_3 and $CaAl_4O_7$ (grossite), together with Fe,Mg-bearing oxides (Fig. 5). The $CaAl_4O_7$ partially surrounds the Al_2O_3 and may have formed by reaction of this grain with the stellar gas as temperatures dropped (Lodders and Fegley 1999). The Fe,Mg-oxides, in turn, partially surround the $CaAl_4O_7$, forming a sequence of increasingly less refractory grains from the upper right to the lower left of the grain as shown in Fig. 5. This complex grain shows heterogeneity in its O isotopic composition, with less anomalous O in the Fe,Mg-oxides than in the Al-bearing oxides. Despite this heterogeneity, it is likely that all the sub-components also formed in the same stellar environment from a gas with a uniform O isotopic composition. As discussed more extensively below, the presence of Fe-rich rims around both of these complex grains suggests infiltration of Fe into the grains due to secondary alteration. The less anomalous O isotopic compositions of the Fe,Mg-oxides are probably due to partial re-equilibration of the grains with isotopically normal O from the surrounding matrix during this process. Dilution of the most anomalous region (area 1 in Table 1) in complex grain 3a-1-o2 with 45% solar composition oxygen can reproduce the O isotopic compositions of the least anomalous region (area 3 in Table 1); 33% dilution is required to reproduce the O isotopic composition of area 2.

Presolar Grain Abundances

Kakangari, as noted above, has upper limits of approximately 4–5 ppm for both SiC and presolar silicates and oxides. For Adelaide, the calculated abundance of all O-anomalous grains in our inventory is 70 ± 10 ppm; the oxide abundance is 17 ± 6 ppm and the silicate abundance is 53 ± 8 ppm. Davidson et al. (2010) obtained a significantly higher abundance of about 250 ppm for O-anomalous grains in Adelaide. However, their estimate was based on only seven grains in 2600 μm^2 area; as discussed below, presolar grain abundances in this meteorite are very heterogeneous from one matrix area to another and the grains identified by Davidson et al. (2010) appear to be from a presolar grain-rich matrix area. The data from this study, with a

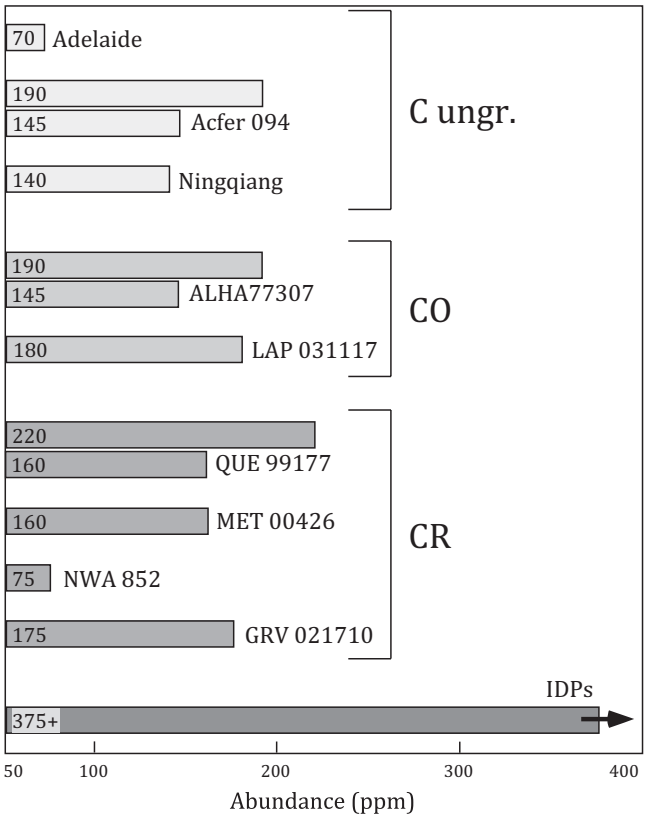

Fig. 6. Matrix-normalized abundances (ppm) of presolar oxides and silicates in Adelaide compared with various carbonaceous chondrites and IDPs. Literature data are from Floss et al. (2006), Nguyen et al. (2007, 2010), Floss and Stadermann (2009a), Vollmer et al. (2009), Leitner et al. (2012), Haenecour and Floss (2011), Zhao et al. (2011), Bose et al. (2012).

higher number of grains identified and a much larger area measured, are more representative of Adelaide as a whole. The abundance we obtain for Adelaide is lower by a factor of 2–3 than the presolar silicate and oxide abundances of other highly primitive carbonaceous chondrites, which are generally between 150 and 200 ppm (Fig. 6). Abundances in IDPs are even higher, with minimum values of about 375 ppm for the most primitive IDPs (Messenger et al. 2003; Floss et al. 2006; Busemann et al. 2009). The CR2 chondrite NWA 852 also has relatively low O-anomalous grain abundances, approximately 75 ppm (Fig. 6). Leitner et al. (2012) suggested that NWA 852 may have lost some presolar grains due to the aqueous alteration it has experienced, and that this meteorite might represent a link between nearly pristine CR3 chondrites like QUE 99177 and MET 00426 (Floss and Stadermann 2009a) and other CR chondrites, which have lower presolar grain abundances (e.g., Nagashima et al. 2004). Floss and Stadermann (2009a) suggested that the presolar silicate/oxide ratio may be a measure of the degree of alteration experienced by a meteorite, with high silicate/oxide ratios indicative of less processing since oxide grains are expected to be more resistant to secondary processes than silicate grains. This ratio is quite variable in the presolar grain-rich meteorites that have been analyzed to date, with values up to about 22 for IDPs and the CR3 chondrites (Floss and Stadermann 2009a). Leitner et al. (2012) calculated a theoretical value of about 23 for the silicate/oxide ratio of dust from AGB stars, suggesting that the presolar silicate and oxide abundances observed in the CR3 chondrites and IDPs reflect their initial abundances in the regions of the solar nebula where the parent bodies of these samples formed. NWA 852, however, has a very low silicate/oxide ratio of about 2, consistent with destruction of some silicates through aqueous alteration (Leitner et al. 2012). The presolar silicate/oxide ratio of Adelaide is also very low, about 3; this together with the lower abundance of O-anomalous grains, suggests that secondary processing has destroyed some fraction of the presolar silicate inventory of Adelaide.

Our calculated SiC abundance in Adelaide is 8 ± 3 ppm; this estimate includes only those grains that were positively identified as SiC (Table 4). Davidson et al. (2010) determined an abundance of 23 ppm, based on a single grain; within errors this is consistent with our estimate. This abundance is within the range of SiC abundances determined for a series of carbonaceous chondrites based on noble gas measurements (Huss et al. 2003), but is about an order of magnitude lower than recent estimates based on NanoSIMS ion imaging measurements (up to approximately 100 ppm; Floss and Stadermann 2009c; Bose et al. 2012; Leitner et al. 2012). Presolar SiC is more resistant to secondary processing than some other presolar phases, particularly silicates. For example, Davidson et al. (2009) showed that SiC abundances do not vary significantly with the degree of aqueous alteration in CR chondrites, whereas presolar silicate abundances are affected (Nagashima et al. 2004; Leitner et al. 2012). However, Huss et al. (2003) argued that thermal metamorphism does affect SiC abundances and have used differences in abundance to estimate the degree of nebular processing experienced by different chondrite groups. If this is the case, then the low SiC abundance of Adelaide suggests that it has experienced significant thermal processing. As noted above, NanoSIMS ion imaging studies, for the most part, indicate higher SiC abundances than the noble gas studies of Huss and Lewis (1995) and Huss et al. (2003); however, these investigations have focused only on meteorites of low petrologic type. Similar NanoSIMS measurements on meteorites of higher petrologic type could help determine whether SiC is, indeed, destroyed

at higher temperatures or has simply lost some of its noble gas inventory, as suggested by Davidson et al. (2009).

Presolar grain abundances are also highly variable within Adelaide; three different matrix regions (7, 3, and 5) have O-anomalous grain abundances that vary from about 30 ppm (one grain, 8000 μm^2) to about 95 ppm (20 grains, 7300 μm^2) to about 175 ppm (24 grains, 6400 μm^2), respectively. Areas 3 and 5, with the highest abundances of O-anomalous grains, also contain the most C-anomalous grains (five grains each). In other matrix regions the number of grains identified is low, but the amount of area measured ($\leq\sim$2000 μm^2) is not sufficient to provide statistically meaningful abundance estimates. Examination of the matrix areas clearly shows that the difference in presolar grain abundances is correlated with grain size (Fig. 7). The matrix in area 5 is fine-grained, with grain sizes typically one micrometer or less, whereas area 7 is significantly more coarse grained. Similar heterogeneities in presolar grain abundances have been observed in other meteorites, for example QUE 99177 (Floss and Stadermann 2009a), but the difference is more pronounced in Adelaide. Moreover, unlike Adelaide, the matrix material in QUE 99177 did not show any obvious petrographic differences between matrix areas with different presolar grain abundances. The coarser grain size of the matrix from area 7 suggests that this material has experienced recrystallization and grain growth, probably in response to elevated temperatures. This process is likely also responsible for the low presolar grain abundance in this area; the single presolar grain that was identified is an oxide grain and is the largest presolar grain found in our study (Table 1). These features probably account for its survival relative to presolar silicates, which are generally smaller and more labile. The ungrouped C chondrite Ningqiang also shows a strongly heterogeneous distribution of O-anomalous grains, with larger average grain sizes in the matrix areas that are presolar grain-depleted (Zhao et al. 2011b).

Elevated Fe Abundances in Adelaide Presolar Silicates

One of the early surprises after the initial discovery of presolar silicates was that the vast majority of these grains had higher Fe contents than expected based on equilibrium condensation calculations (e.g., Lodders and Fegley 1999) and astronomical observations (e.g., Waters et al. 1996; Demyk et al. 2000), which predicted Mg-rich silicates. Whether these high Fe contents are a primary signature of the presolar grains or the result of secondary alteration has been extensively discussed in the literature (e.g., Floss and Stadermann 2009a; Vollmer et al. 2009; Bose et al. 2010a; Nguyen et al. 2010). Although secondary alteration may have played some role (e.g.,

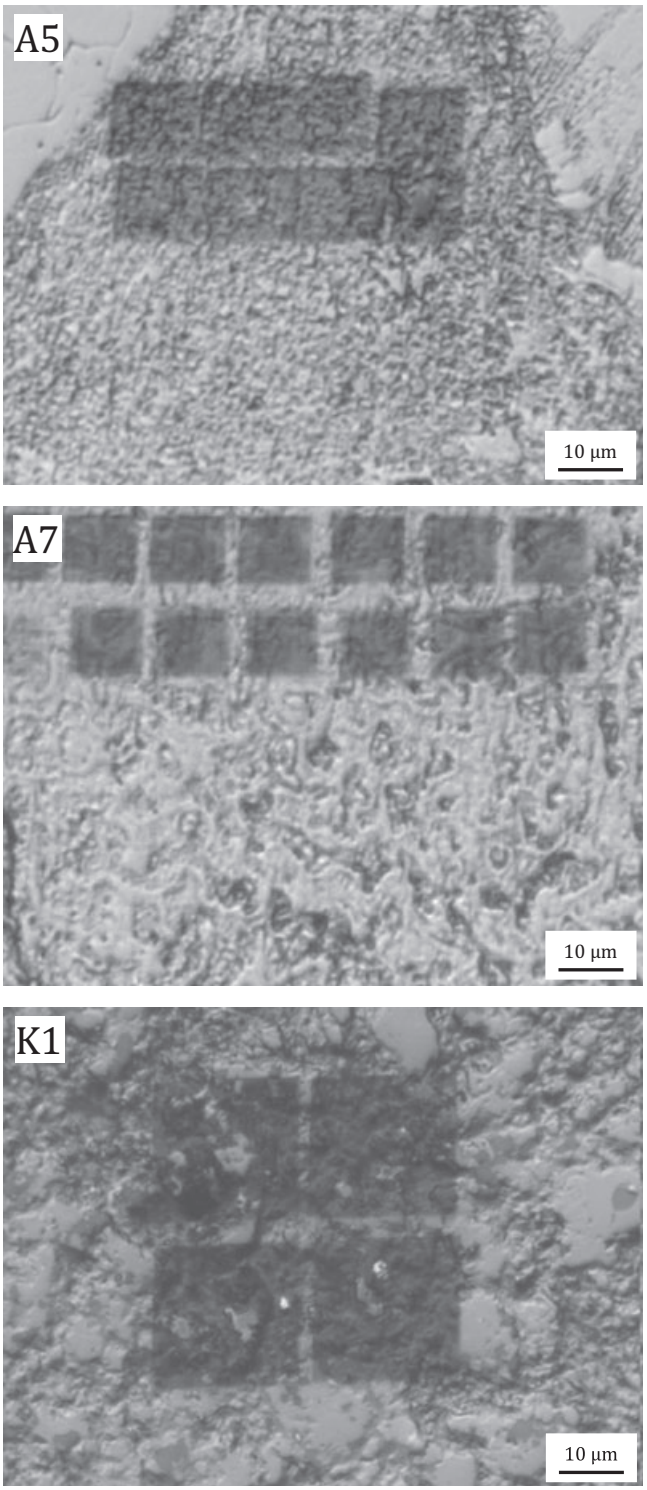

Fig. 7. Reflected light images of matrix areas 7 and 5 in Adelaide (A5 and A7) and matrix area 1 in Kakangari (K1). Note that the scale is the same in all three images, but that the NanoSIMS raster imaging areas (dark squares) are 10×10 μm^2 in Adelaide and 20×20 μm^2 in Kakangari. Area 7 in Adelaide has a coarser grain size and significantly lower presolar grain abundances than area 5; grain size is coarsest in the matrix of Kakangari.

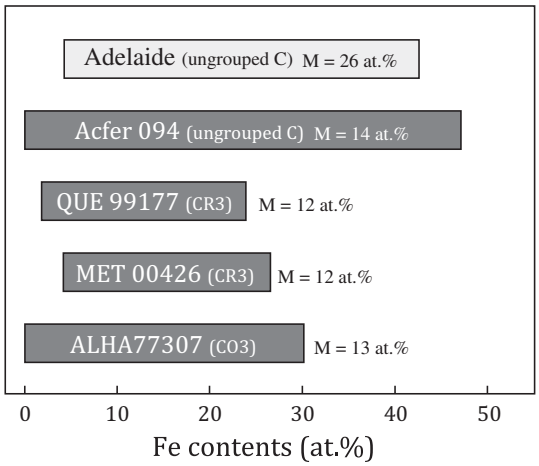

Fig. 8. Range of Fe contents in presolar silicate grains from Adelaide and other carbonaceous chondrites. The median values (M) for each meteorite are also shown. Literature data are from Floss and Stadermann (2009a), Vollmer et al. (2009), Bose et al. (2010a, 2012), Nguyen et al. (2010).

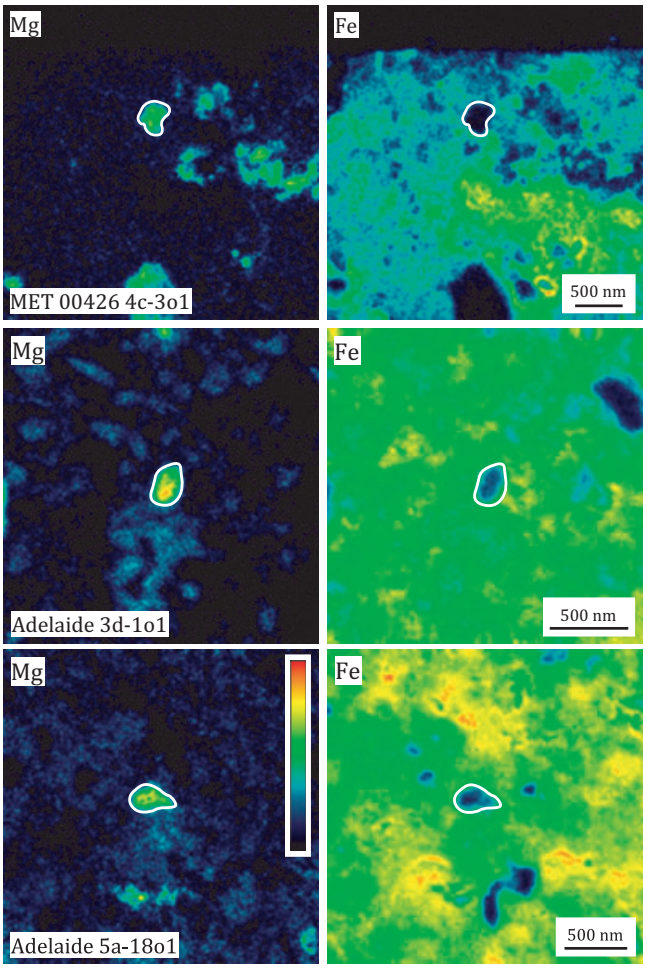

Fig. 9. False-color Mg and Fe distribution maps of presolar silicates from Adelaide and the MET 00426 CR3 chondrite.

Bose et al. 2010a), the ubiquitous presence of Fe-rich presolar silicates in meteorites that have experienced very little secondary processing (e.g., Floss and Stadermann 2009a; Nguyen et al. 2010) argues for a primary origin for much of the Fe in these grains. Iron isotopic measurements can provide a definitive test and, indeed, several presolar grains from Acfer 094 have nonsolar Fe isotopic compositions (Mostefaoui and Hoppe 2004; Floss et al. 2008; Vollmer and Hoppe 2010; Ong et al. 2012), indicating primary Fe in these grains. A number of other presolar silicates have solar Fe isotopic ratios (e.g., Vollmer and Hoppe 2010; Ong et al. 2012), but the significance of these results is not clear, as the measurements are difficult to carry out and errors are typically large.

Figure 8 shows the range of Fe contents in presolar silicates from different primitive chondrites; abundances typically range up to about 30 atom%. The presolar silicates in Adelaide, however, have even higher Fe contents, with abundances up to about 40–45 atom%. Presolar silicates in Acfer 094 are also very Fe-rich, with a range greater than those of Adelaide. However, the median Fe content of Adelaide is significantly higher (26 atom%) than that of Acfer 094 (14 atom%) or the other primitive carbonaceous chondrites (12–13 atom%). In addition, Fig. 2 shows that in Acfer 094 most of the grains have compositions that are similar to either olivine or pyroxene, or fall between the two; this is also true for the presolar silicates in most other meteorites (e.g., Floss and Stadermann 2009a; Vollmer et al. 2009; Bose et al. 2010b; Nguyen et al. 2010). The situation is very different for the presolar silicates in Adelaide: four grains have compositions similar to olivine and one grain has a composition similar to pyroxene, but all other grains in Adelaide have (Mg + Fe)/Si ratios that are significantly higher than that of olivine (Fig. 2). Cation/O ratios are also significantly elevated in many of the presolar silicates from Adelaide (0.66–1.35, with most >0.80; Table 2) compared to a range of 0.59–0.97 for presolar silicates from other primitive meteorites (e.g., Floss and Stadermann 2009a; Vollmer et al. 2009).

Moreover, as we noted above, the two complex grains found in Adelaide have Fe-rich rims that seem to suggest diffusion of Fe into the grains. We see similar rims around some of the individual presolar grains in Adelaide. Figure 9 shows two such presolar silicates with clear rims of Fe penetrating the grains, compared with a presolar silicate from the MET 00426 CR3 chondrite, where no such rim is present. Taken together, our observations suggest that at least some fraction of the Fe in the presolar silicates from Adelaide is due to secondary alteration. The Fe-rich rims indicate infusion

of Fe into the grains from the surrounding matrix, resulting in elevated Fe contents and, consequently, elevated Mg + Fe/Si and cation/O ratios compared to most presolar silicates from other primitive chondrites. Diffusion, strictly defined, is an exchange process, but in these grains we see a clear net addition of Fe into the grains, suggesting a kinetic process rather than equilibrium diffusion. Although we do not have structural information on these grains, it is likely that many of them are amorphous and this may also facilitate infusion of Fe into the grains.

Secondary Processing in Adelaide and Kakangari

Our study shows that both Adelaide and Kakangari have lower presolar grain abundances than Acfer 094 and ALHA77307 and, therefore, seem to be less primitive. The matrix of Kakangari is Mg-rich and is dominated by structurally and mineralogically distinct aggregates of crystalline enstatite and olivine, with lesser amounts of albite, anorthite, spinel, troilite, and Fe,Ni metal; amorphous silicates are essentially absent (Brearley 1989). Matrix textures and enstatite microstructures indicate high-temperature (>1000 °C) processing with rapid cooling, but melting does not seem to have occurred. Moreover, Berlin et al. (2007) showed that chondrules as well as other components in Kakangari have experienced wide-spread reduction, which probably took place both in the nebula at the time of chondrule formation and later on the parent body. The matrix mineralogy of Kakangari probably formed through high-temperature reaction of fine-grained amorphous or partially crystalline dust, in a thermal event similar to the one that formed chondrules. Such processing will destroy presolar silicates, as well as other presolar grains (e.g., Huss and Lewis 1995; Huss et al. 2003), accounting for the paucity of presolar grains in this meteorite.

Although ungrouped, Adelaide shows similarities to the CO3 chondrite ALHA77307, such as matrix abundance, mineralogy, and chondrule size; both meteorites are also highly un-equilibrated (Brearley 1991). However, there are also important differences. Olivines in the matrix of Adelaide are significantly more fayalitic than the Mg-rich ones typically seen in ALHA77307 (Brearley 1993) and bulk analyses of the Adelaide matrix show that it is more Fe-rich than chondrite matrices in general. In addition, although both meteorites contain amorphous material in their matrices, the matrix of Adelaide is more crystalline than that of ALHA77307, suggesting that it has experienced some thermal annealing (Brearley 1991). Adelaide is also highly weathered, with extensive replacement of metal and sulfides by goethite (Davy et al. 1978). Terrestrial weathering has been shown to remove Mg and Si from ordinary chondrites, but Fe abundances appear to be unaffected (Bland et al. 1998). In contrast thermal metamorphism can result in increased Fe contents in originally Mg-rich grains (Jones and Rubie 1991). Annealing of Adelaide matrix material is, therefore, probably responsible for the elevated Fe contents in its presolar silicates, with Fe permeating into the grains from the surrounding Fe-rich matrix. This process does not require that all Fe in the presolar silicates is secondary. Indeed, as noted earlier, the fact that Fe contents are high in presolar silicates from all primitive meteorites argues for incorporation of at least some Fe into the grains during formation in their stellar environments (Floss and Stadermann 2009a; Vollmer et al. 2009; Bose et al. 2010a, 2012; Nguyen et al. 2010).

Lower presolar grain abundances in Adelaide compared to other primitive carbonaceous chondrites (Fig. 6) and dilution of the O isotopes in some parts of complex grain 3a-1-o2 (Fig. 4) are also consistent with thermal processing. However, if the lower presolar grain abundances are due to parent body thermal metamorphism, we would expect to see uniform depletions throughout the meteorite. Instead, as noted earlier, the distributions of both O-anomalous and C-anomalous presolar grains are highly heterogeneous among different matrix areas in Adelaide, with most of the presolar grains present in only two of the nine matrix areas studied. One possibility is that the extensive terrestrial weathering experienced by Adelaide has destroyed some of the presolar silicates. This type of alteration would be consistent with the heterogeneous distribution of these grains, as weathering is likely to act variably in different parts of the meteorite. However, presolar SiC abundances also differ among the different matrix areas, but are probably resistant to terrestrial alteration, as these grains survive even the harsh acid treatments traditionally used to separate them from their host meteorites (Amari et al. 1994). Moreover, there are no obvious petrographic features in our thin section indicative of localized weathering, such as the preferential occurrence of alteration veins near the presolar grain-poor matrix areas.

Instead, as noted earlier, the primary difference between matrix areas rich in presolar grains and those poor in presolar grains is grain size (Fig. 7). Areas poor in presolar grains have a coarser average grain size than areas rich in presolar grains, probably as a result of recrystallization and grain growth during heating. The close proximity of matrix areas with different grain sizes, and different presolar grain abundances, suggests that this thermal processing was highly variable. Short-lived high temperature events, like those thought to be responsible for the formation of chondrules (Bally et al. 2005), will also process fine-grained dust in the nebula

(Nuth et al. 2005). Such events may be highly localized, with different effects on different parcels of gas and dust, leading to grain coarsening and the destruction of presolar grains in some material, but not in others. Brearley (1991) noted that most matrix components in ALHA77307 are also found in Adelaide, only in very different modal abundances, and suggested that sampling of poorly mixed material could account for the observed differences. Similar accretion of materials processed to different degrees may be responsible for the variability observed in Adelaide matrix material. Based on its paucity of presolar grains (one oxide grain in 8000 μm^2 of area 7 measured), the degree of heating and recrystallization experienced by the most coarse-grained matrix area in Adelaide approaches that of the matrix material in Kakangari, in which no presolar grains were found; comparison of the matrix in Adelaide with that in Kakangari supports this suggestion (Fig. 7).

A similar process of short-lived high temperature events may also be responsible for infiltration of Fe from the surrounding matrix, as observed in the presolar silicates and complex grains. However, this would require that heating occurred after aggregation of millimeter- to centimeter-sized clumps of material in order for Fe to enter the presolar grains from surrounding Fe-rich material. Such an environment would be highly oxidizing, due to the local enhancement of dust-to-gas ratios and could be responsible for the overall Fe-rich nature of Adelaide matrix material compared to other chondrites.

Based on the differences between Adelaide and Kakangari, and other primitive chondrites with more presolar grains, it is clear that one of the defining characteristics common to primitive meteorites with high presolar grain abundances is the presence of amorphous silicates. Both Acfer 094 and ALHA77307 are highly un-equilibrated and contain abundant fine-grained Fe- and Si-rich amorphous material in their matrices (Brearley 1993; Greshake 1997). The CR3s QUE 99177 and MET 00426 are very primitive members of the CR chondrite group; unlike other CRs, they contain few crystalline phyllosilicates and their matrices are dominated by fine-grained amorphous silicates (Abreu and Brearley 2010). The new CO3 chondrite LAP 031117 and the CR chondrite GRV 021710 have similarly high presolar grain abundances (Haenecour and Floss 2011; Zhao et al. 2011a), but to date there have not been any detailed investigations of their matric mineralogies. Chizmadia and Cabret-Lebrón (2009) have suggested, on the basis of olivine compositions, that LAP 031117 is very primitive, like ALHA77307. GRV 021710 was classified as a CR2 chondrite (Russell et al. 2005), but a type 3 classification may be more appropriate.

Acknowledgments—Detailed, constructive reviews by P. Hoppe, L. Nittler, and an anonymous reviewer provided useful improvements and are appreciated. This work was supported by NASA grant NNX10AH43G.

Editorial Handling—Dr. Adrian Brearley

REFERENCES

Abreu N. M. and Brearley A. J. 2010. Early solar system processes recorded in the matrices of two highly pristine CR3 carbonaceous chondrites, MET 00426 and QUE 99177. *Geochimica et Cosmochimica Acta* 74:1146–1171.

Amari S., Lewis R. S., and Anders E. 1994. Interstellar grains in meteorites. I-Isolation of SiC, graphite, and diamond; size distributions of SiC and graphite. *Geochimica et Cosmochimica Acta* 58:459–470.

Amari S., Nittler L. R., Zinner E., Lodders K., and Lewis R. S. 2001. Presolar SiC grains of type A and B: Their isotopic compositions and stellar origins. *The Astrophysical Journal* 559:463–483.

Bally J., Moeckel N., and Throop H. 2005. Evolution of UV-irradiated protoplanetary disks. In *Chondrites and the protoplanetary disk*, edited by Krot A. N., Scott E. R. D., and Reipurth B. San Francisco, CA: Astronomical Society of the Pacific. pp. 81–106.

Berlin J., Jones R. H., and Brearley A. J. 2007. A closer look at chondrules and matrix in Kakangari: Evidence for wide-spread reduction and sulfurization (abstract #2395). 38th Lunar and Planetary Science Conference. CD-ROM.

Bland P. A., Sexton A. S., Jull A. J. T., Bevan A. W. R., Berry F. J., Thornley D. M., Astin T. R., Britt D. T., and Pillinger C. T. 1998. Climate and rock weathering: A study of terrestrial age dated ordinary chondritic meteorites from hot desert regions. *Geochimica et Cosmochimica Acta* 62:3169–3184.

Boothroyd A. I. and Sackmann I. J. 1999. The CNO isotopes: Deep circulation in red giants and first and second dredge-up. *The Astrophysical Journal* 510:232–250.

Bose M., Floss C., and Stadermann F. J. 2010a. An investigation into the origin of Fe-rich presolar silicates in Acfer 094. *The Astrophysical Journal* 714:1624–1636.

Bose M., Zhao X., Floss C., Stadermann F. J., and Lin Y. 2010b. Stardust material in the paired enstatite meteorites: SAH 97096 and SAH 97159. Proceedings, 11th Symposium on Nuclei in the Cosmos. p. 138.

Bose M., Floss C., Stadermann F. J., Stroud R. M., and Speck A. K. 2012. Stellar and interstellar material in the CO3 chondrite ALHA77307: An isotopic and elemental investigation. *Geochimica et Cosmochimica Acta*, forthcoming.

Brearley A. J. 1989. Nature and origin of matrix in the unique type 3 chondrite, Kakangari. *Geochimica et Cosmochimica Acta* 53:2395–2411.

Brearley A. J. 1991. Mineralogical and chemical studies of matrix in the Adelaide meteorite, a unique carbonaceous chondrite with affinities to ALH77307 (CO3) (abstract). 22nd Lunar and Planetary Science Conference. p. 133.

Brearley A. J. 1993. Matrix and fine-grained rims in the unequilibrated CO3 chondrite, ALHA77307: Origins and evidence for diverse, primitive nebular dust components. *Geochimica et Cosmochimica Acta* 57:1521–1550.

Busemann H., Nguyen A. N., Cody G. D., Hoppe P., Kilcoyne A. L. D., Stroud R. M., Zega T. J., and Nittler L. R. 2009. Ultra-primitive interplanetary dust particles from the comet 26P/Grigg-Skjellerup dust stream collection. *Earth and Planetary Science Letters* 288:44–57.

Chizmadia L. J. and Cabret-Lebrón E. 2009. LaPaz 031117: A new primitive CO3 carbonaceous chondrite (abstract #2031). 40th Lunar and Planetary Science Conference. CD-ROM.

Davidson J., Busemann H., Alexander C. M. O'D., Nittler L. R., Schrader D. L., Orthous-Daunay F. R., Quirico E., Franchi I. A., and Grady M. M. 2009. Presolar SiC abundances in primitive meteories by NanoSIMS raster ion imaging of insoluble organic matter (abstract #1853). 40th Lunar and Planetary Science Conference. CD-ROM.

Davidson J., Busemann H., Franchi I. A., and Grady M. M. 2010. Presolar grain inventories of the ungrouped C3 Adelaide and the CV3 RBT 04133 (abstract #2230). 41st Lunar and Planetary Science Conference. CD-ROM.

Davy R., Whitehead S. G., and Pitt G. 1978. The Adelaide meteorite. *Meteoritics* 13:121–140.

Demyk K., Dartois E., Wiesemeyer H., Jones A. P., and d'Hendecourt L. 2000. Structure and chemical composition of the silicate dust around OH/IR stars. *Astronomy & Astrophysics* 364:170–178.

Ferrarotti A. S. and Gail H.-P. 2001. Mineral formation in stellar winds II. Effects of Mg/Si abundance variations on dust composition in AGB stars. *Astronomy & Astrophysics* 371:133–151.

Floss C. and Stadermann F. J. 2009a. Auger Nanoprobe analysis of presolar ferromagnesian silicate grains from primitive CR chondrites QUE 99177 and MET 00426. *Geochimica et Cosmochimica Acta* 73:2415–2440.

Floss C. and Stadermann F. J. 2009b. The presolar grain inventories of Adelaide and Kakangari (abstract). *Geochimica et Cosmochimica Acta* 73:A385.

Floss C. and Stadermann F. J. 2009c. High abundances of circumstellar and interstellar C-anomalous phases in the primitive CR3 chondrites QUE 99177 and MET 00426. *The Astrophysical Journal* 697:1242–1255.

Floss C., and Stadermann F. J. 2010. Presolar silicate and oxide grains in the ungrouped carbonaceous chondrite Adelaide: Effects of thermal annealing (abstract #1251). 41st Lunar and Planetary Science Conference. CD-ROM.

Floss C. Stadermann F. J., Bradley J. P., Dai Z. R., Bajt S., and Graham G. 2004. Carbon and nitrogen isotopic anomalies in an anhydrous interplanetary dust particle. *Science* 303:1355–1358.

Floss C., Stadermann F. J., Bradley J. P., Dai Z. R., Bajt S., Graham G., and Lea A. S. 2006. Identification of isotopically primitive interplanetary dust particles: A NanoSIMS isotopic imaging study. *Geochimica et Cosmochimica Acta* 70:2371–2399.

Floss C., Stadermann F. J., and Bose M. 2008. Circumstellar Fe oxide from the Acfer 094 carbonaceous chondrite. *The Astrophysical Journal* 672:1266–1271.

Floss C., Stadermann F. J., Mertz A. F., and Bernatowicz T. 2010. A NanoSIMS and Auger Nanoprobe investigation of an isotopically primitive interplanetary dust particle from the 55P/Tempel-Tuttle targeted stratospheric dust collector. *Meteoritics & Planetary Science* 45:1889–1905.

Gail H.-P. and Sedlmayr E. 1999. Mineral formation in stellar winds I. Condensation sequence of silicate and iron grains in stationary oxygen rich outflows. *Astronomy & Astrophysics* 347:594–616.

Gail H.-P., Zhukovska S. V., Hoppe P., and Trieloff M. 2009. Stardust from asymptotic giant branch stars. *The Astrophysical Journal* 698:1136–1154.

Greshake A. 1997. The primitive matrix components of the unique carbonaceous chondrite Acfer 094: A TEM study. *Geochimica et Cosmochimica Acta* 61:437–452.

Gyngard F., Zinner E., Nittler L., Morgand A., Stadermann F. J., and Hynes K. M. 2010. Automated NanoSIMS measurements of spinel stardust from the Murray meteorite. *The Astrophysical Journal* 717:107–120.

Gyngard F., Nittler L. R., Zinner E., José J., and Cristallo S. 2011. New reaction rates and implications for nova nucleosynthesis and presolar grains (abstract #2675). 42nd Lunar and Planetary Science Conference. CD-ROM.

Haenecour P. and Floss C. 2011. High abundance of stardust in the CO3.0 chondrite LaPaz 031117 (abstract). *Meteoritics & Planetary Science* 46:A85.

Huss G. R. and Lewis R. S. 1995. Presolar diamond, SiC, and graphite in primitive chondrites: Abundances as a function of meteorite class and petrologic type. *Geochimica et Cosmochimica Acta* 59:115–160.

Huss G. R., Meshik A. P., Smith J. B., and Hohenberg C. 2003. Presolar diamond, silicon carbide, and graphite in carbonaceous chondrites: Implications for thermal processing in the solar nebula. *Geochimica et Cosmochimica Acta* 67:4823–4848.

Hutchison R. 2004. *Meteorites: A petrologic, chemical and isotopic synthesis*. London: Cambridge University Press. 524 p.

Iliadis C., Angulo C., Descouvemont P., Lugaro M., and Mohr P. 2008. New reaction rate for $^{16}O(p,y)^{17}F$ and its influence on the oxygen isotopic ratios in massive AGB stars. *Physical Review C* 77: 045802-1–045802-11, doi:045802.

Jones R. H. and Rubie D. C. 1991. Thermal histories of CO3 chondrites: Application of olivine diffusion modeling to parent body metamorphism. *Earth and Planetary Science Letters* 106:73–86.

José J., Hernanz M., Amari S., Lodders K., and Zinner E. 2004. The imprint of nova nucleosynthesis in presolar grains. *The Astrophysical Journal* 612:414–428.

Leitner J., Vollmer C., Hoppe P., and Zipfel J. 2012. Characterization of presolar material in the CR chondrite Northwest Africa 852. *The Astrophysical Journal* 745:38, doi:10.1088/0004-637X/745/1/38.

Lodders K. and Fegley B. 1999. Condensation chemistry of circumstellar grains. In *Asymptotic giant branch stars*, edited by Le Berre T., Lebre A., and Waelkens C. San Francisco, CA: Astronomical Society of the Pacific. pp. 279–289.

Maldoni M. M., Ireland T. R., and Robinson G. 2008. IRAS 22036 + 5306: An Al_2O_3 oxide-dominated post-AGB star. *Monthly Notices of the Royal Astronomical Society* 386:2290–2296.

Messenger S., Keller L. P., Stadermann F. J., Walker R. M., and Zinner E. 2003. Samples of stars beyond the solar system: Silicate grains in interplanetary dust. *Science* 300:105–108.

Mostefaoui S. and Hoppe P. 2004. Discovery of abundant *in situ* silicate and spinel grains from red giant stars in a primitive meteorite. *The Astrophysical Journal* 613:L149–L152.

Nagashima K., Krot A. N., and Yurimoto H. 2004. Stardust silicates from primitive meteorites. *Nature* 428:921–924.

Nguyen A. N. and Zinner E. 2004. Discovery of ancient silicate stardust in a meteorite. *Science* 303:1496–1499.

Nguyen A. N., Stadermann F. J., Zinner E., Stroud R. M., Alexander C. M. O'D., and Nittler L. R. 2007. Characterization of presolar silicate and oxide grains in primitive carbonaceous chondrites. *The Astrophysical Journal* 656:1223–1240.

Nguyen A. N., Nittler L., Stadermann F. J., Stroud R., and Alexander C. M. O'D. 2010. Coordinated analyses of presolar grains in the Allan Hills 77307 and Queen Elizabeth Range 99177 meteorites. *The Astrophysical Journal* 719:166–189.

Nittler L. R. 2009. On the mass and metallicity distributions of the parent AGB stars of O-rich presolar stardust grains. *Publications of the Astronomical Society of Australia* 26:271–277.

Nittler L. R. and Hoppe P. 2005. Are presolar silicon carbide grains from novae actually from supernovae? *The Astrophysical Journal* 631:L89–L92.

Nittler L. R., Alexander C. M. O'D., Gao X., Walker R. M., and Zinner E. 1997. Stellar sapphires: The properties and origins of presolar Al_2O_3 in meteorites. *The Astrophysical Journal* 483:475–495.

Nittler L. R., Alexander C. M. O'D., Gallino R., Hoppe P., Nguyen A. N., Stadermann F. J., and Zinner E. K. 2008. Aluminum-, calcium- and titanium-rich oxide stardust in ordinary chondrite meteorites. *The Astrophysical Journal* 682:1450–1478.

Nuth J. A., Brearley A. J., and Scott E. R. D. 2005. Microcrystals and amorphous material in comets and primitive meteorites: keys to understanding processes in the early solar system. In *Chondrites and the protoplanetary disk*, edited by Krot A. N., Scott E. R. D., and Reipurth B. San Francisco, CA: Astronomical Society of the Pacific. pp. 675–700.

Ong W. J., Floss C., and Gyngard F. 2012. Negative secondary ion measurements of $^{54}Fe/^{56}Fe$ and $^{57}Fe/^{56}Fe$ in presolar silicate grains from Acfer 094 (abstract #1225). 43rd Lunar and Planetary Science Conference. CD-ROM.

Russell S. S., Zolensky M. E., Righter K., Folco L., Jones R. H., Connolly H. C., Grady M. M., and Grossman J. N. 2005. The Meteoritical Bulletin, No. 89, 2005 September. *Meteoritics & Planetary Science* 40:A201–A263.

Scott E. R. D. and Krot A. N. 2005. Thermal processing and accretion of silicate dust into chondrites and comets (abstract #2007). 36th Lunar and Planetary Science Conference. CD-ROM.

Sloan G. C., Kraemer K. E., Goebel J. H., and Price S. D. 2003. Guilt by association: The 13 micron dust emission feature and its correlation to other gas and dust features. *The Astrophysical Journal* 594:483–495.

Stadermann F. J., Floss C., Bose M., and Lea A. S. 2009. The use of Auger spectroscopy for the *in situ* elemental characterization of sub-micrometer presolar grains. *Meteoritics & Planetary Science* 44:1033–1049.

Stroud R. M., Floss C., and Stadermann F. J. 2009. Structure, elemental composition and isotopic composition of presolar silicates in MET 00426 (abstract #1063). 40th Lunar and Planetary Science Conference. CD-ROM.

Toppani A., Libourel G., Robert F., and Ghanbaja J. 2006. Laboratory condensation of refractory dust in protosolar and circumstellar conditions. *Geochimica et Cosmochimica Acta* 70:5035–5060.

Vollmer C. and Hoppe P. 2010. First Fe isotopic measurement of a highly ^{17}O-enriched stardust silicate (abstract #1200). 41st Lunar and Planetary Science Conference. CD-ROM.

Vollmer C., Hoppe P., and Brenker F. E. 2008. Si isotopic compositions of presolar silicate grains from red giant stars and supernovae. *The Astrophysical Journal* 684: 611–617.

Vollmer C., Brenker F., Hoppe P., and Stroud R. 2009a. Direct laboratory analysis of silicate stardust from red giant stars. *The Astrophysical Journal* 700:774–782.

Vollmer C., Hoppe P., Stadermann F. J., Floss C., and Brenker F. E. 2009b. NanoSIMS analysis and Auger electron microscopy of silicate and oxide stardust from the carbonaceous chondrite Acfer 094. *Geochimica et Cosmochimica Acta* 73:7127–7149.

Waters L. B. F. M., Molster F. J., de Jong T., Beintema D. A., Waelkens C., Boogert A. C. A., Boxhoorn D. R., de Graauw T., Drapatz S., Feuchtgruber H., Genzel R., Helmich F. P., Heras A. M., Huygen R., Izumiura H., Justtanont K., Kester D. J. M., Kunze D., Lahuis F., Lamers H. J. G. L. M., Leech K. J., Loup C., Lutz D., Morris P. W., Price S. D., Roelfsema P. R., Salama A., Schaeidt S. G., Tielens A. G. G. M., Trams N. R., Valentijn E. A., Vandenbussche B., van den Ancker M. E., van Dishoeck E. F., van Winckel H., Wesselius P. R., and Young E. T. 1996. Mineralogy of oxygen-rich dust shells. *Astronomy & Astrophysics* 315:L361–L364.

Wilson T. L. and Rood R. T. 1994. Abundances in the interstellar medium. *Annual Reviews of Astronomy and Astrophysics* 32:191–226.

Yada T., Floss C., Stadermann F. J., Zinner E., Nakamura T., Noguchi T., and Lea A. S. 2008. Stardust in Antarctic micrometeorites. *Meteoritics & Planetary Science* 43:1287–1298.

Zhao X., Floss C., Stadermann F. J., Lin Y., and Bose M. 2011a. The stardust investigation into the CR2 chondrite GRV 021710 (abstract). *Meteoritics & Planetary Science* 46:A261.

Zhao X., Floss C., Stadermann F. J., Bose M., and Lin Y. 2011b. Continued investigation of presolar silicate grains in the carbonaceous chondrite Ningqiang (abstract #1982). 42nd Lunar and Planetary Science Conference. CD-ROM.

Zinner E. 2007. Presolar grains. In *Meteorites, planets and comets*, edited by Holland H. D. and Turekian K. K. Treatise on Geochemistry, vol. 1.02. Oxford: Elsevier. pp. 1–33.